



Article

Seismic Behavior of Precast Prestressed Concrete Frame with Hinge-Relocated Mortise–Tenon Connections

Hanxi Zhao *  and Noriyuki Takahashi * 

Graduate School of Engineering, Department of Architecture and Building Science, Tohoku University,
Sendai 980-8579, Miyagi, Japan

* Correspondence: zhao.hanxi.s6@dc.tohoku.ac.jp (H.Z.); noriyuki.takahashi.a5@tohoku.ac.jp (N.T.)

Abstract: To satisfy the easy-construction demands of precast concrete (PCa) frames after an earthquake, a PCa frame with mortise–tenon (MT) connections is proposed in this paper. MT connections are secured solely through the binding force of unbonded prestressed tendons without grouting for easy construction. The design and construction of the joint are detailed. During an earthquake, the hinge system of the connection allows for slight rotational movements. Finite element analysis was employed to assess the joint's hysteresis behavior, revealing a three-stage earthquake response mechanism: closing, hinge relocation, and self-centering. Based on the hysteresis performance of the beam and column in the precast prestressed concrete (PCaPC) frame, a seismic response model for PCaPC buildings was established.

Keywords: PCaPC frame; mortise–tenon connection; hinge relocation; finite element analysis



Citation: Zhao, H.; Takahashi, N. Seismic Behavior of Precast Prestressed Concrete Frame with Hinge-Relocated Mortise–Tenon Connections. *Buildings* **2024**, *14*, 3007. <https://doi.org/10.3390/buildings14093007>

Academic Editor: Hugo Rodrigues

Received: 5 August 2024

Revised: 9 September 2024

Accepted: 19 September 2024

Published: 22 September 2024



Copyright: © 2024 by the authors. Licensee MDPI, Basel, Switzerland. This article is an open access article distributed under the terms and conditions of the Creative Commons Attribution (CC BY) license (<https://creativecommons.org/licenses/by/4.0/>).

1. Introduction

Precast concrete construction is characterized by its prominent features of rapid construction and the ability to mechanize on-site operations with a minimal workforce [1–3]. Compared to cast-in situ construction, PCa construction significantly reduces environmental pollution during both the prefabrication and construction phases, resulting in a notable reduction in construction waste generation and carbon emissions. According to statistics from the Ministry of Housing and Urban–Rural Development of China [4–6], in 2021, the total area of newly initiated prefabricated construction in China reached 740 million square meters, representing an 18% increase compared to the year 2020. By 2025, the total area of PCa construction in China is projected to reach 1.651 billion square meters, with the market size expected to reach USD 500 billion. However, the development of PCa construction has been constrained by its high initial construction costs.

The complexity and lack of repetitiveness in the design of prefabricated components have led to a heavy reliance on skilled construction personnel, thereby substantially increasing production and labor costs [7–9]. In many developing countries, the assembly rates for PCa construction typically range between 20% and 50%, with cast-in situ methods still prevalent for beam–column connections during the construction process. Furthermore, as assembly rates increase, incremental costs rise significantly, impeding the progress of fully prefabricated buildings [10–14].

Generally, PCa construction for seismic systems can be broadly classified into emulative and jointed construction [15]. Emulative construction is similar to cast-in situ RC structures regarding lateral strength, stiffness, and energy dissipation. It relies on the plastic deformation of concrete members to dissipate seismic energy. The damaged regions cannot be quickly replaced after earthquakes, resulting in high repair costs for the overall structure. Jointed construction uses precast connection concepts that are distinctly different from emulative connections. Many researchers have proposed various PCaPC jointed constructions, mainly replaceable assembled joint forms composed of energy dissipators, such as bolts,

steel bars, and steel plates [16–21]. These prefabricated energy-dissipating devices can be quickly replaced after an earthquake. However, these structures are relatively complex, and the problem of substantial compression damage at the joints still needs to be resolved. In any case, the traditional structural design concept is to dissipate seismic energy at the expense of component damage. This can cause large inelastic deformations of structural components or even irreparable damage, resulting in enormous economic losses [22–28]. In order to improve the seismic resistance of structures and achieve sustainable buildings, the design of high-resilience jointed connections is anticipated [29–32].

Based on the research mentioned above, the PCaPC frame with MT connections was proposed to achieve the objectives of simple construction, low labor cost, and high resilience. Previous research had shown that MT connections can effectively control beam–column joint failure modes [33]. To further explore the effect of MT connections on the seismic behavior of PCaPC frame structures, PCaPC frames and cast-in situ prestressed concrete (PC) frames were studied using finite element analysis. Additionally, based on the results, a seismic response model of the PCaPC frame for PCaPC buildings was established.

2. Construction Method and Cost

2.1. Configuration

The components and their integration within the PCaPC structure used in this research are illustrated in Figure 1 [34,35]. The interaction between the prestressed reinforcement and concrete differs depending on the connection type, as shown in Figure 2a,b. For the beam-to-column connection, partially unbonded prestressed tendons (PTs) are used. After prestressing, these tendons are anchored at the beam ends with mechanical anchorages. In the beam section, the tendons remain unbonded, allowing free sliding, while at the column ends, the PT tendons are bonded with grout, enabling the stress to be effectively transferred along the tendons, ensuring an even distribution of prestress throughout the concrete. For the column-to-column connection, fully unbonded PT tendons are passed through reserved holes and anchored at the top and bottom of the columns. Mechanical anchorages at both ends maintain tendon tension, ensuring precompression and holding the columns together as a unified assembly. The concrete and tendon properties are listed in Tables 1 and 2 and Table 3, respectively.

Compared to other PCaPC frame joints, it differs primarily in the following three aspects:

1. The tendons for beam-to-column joints are partially unbonded. Previous experimental studies [36] have shown that the strain in the PT tendons across a beam will spread within a certain distance due to bond-slip behavior. A structure with bonded PC strands is considered more robust than one with unbonded strands. Therefore, bonded prestressed tendons are placed at the beam ends. The strain of the unbonded tendons distributes uniformly along the tendon and remains within the yield limit until significant deformation occurs. The unbonded prestressed tendons do not bond with the concrete, allowing the beam to undergo slight rotational movements as a rigid body after loading. After the load is removed, the horizontal tensile stress of the prestressed tendons and the self-weight of the upper structure return the structural components to their initial positions.
2. For beam-to-column joints, MT connections are provided on the precast columns for easy construction and a more reliable transfer of the beam's gravity load to the column. MT connections are positioned at points of zero or small bending moments. This helps the seismic damping mechanism of the structure to function at lower stress levels. During an earthquake, the structure can reduce its rigidity earlier through elastic deformation to implement the hinge-relocation mechanism, thereby reducing the impact on columns and other critical structural parts. Previous studies have included theoretical calculations and validation through finite element simulation of the connection's location.

3. Besides grouting the sheath duct in the column, as shown in Figure 2c,d, the structure does not require cast-in situ construction [37]. Most PCaPC joints in the literature require cast-in situ operations to be performed at the nodes or beam ends. As the assembly rate increases, the incremental cost of PCa buildings also rises. The PCaPC frame with MT connections reduces on-site cast-in situ construction. Without increasing costs, it enhances the assembly rate of the structure and simplifies construction at complex joints.

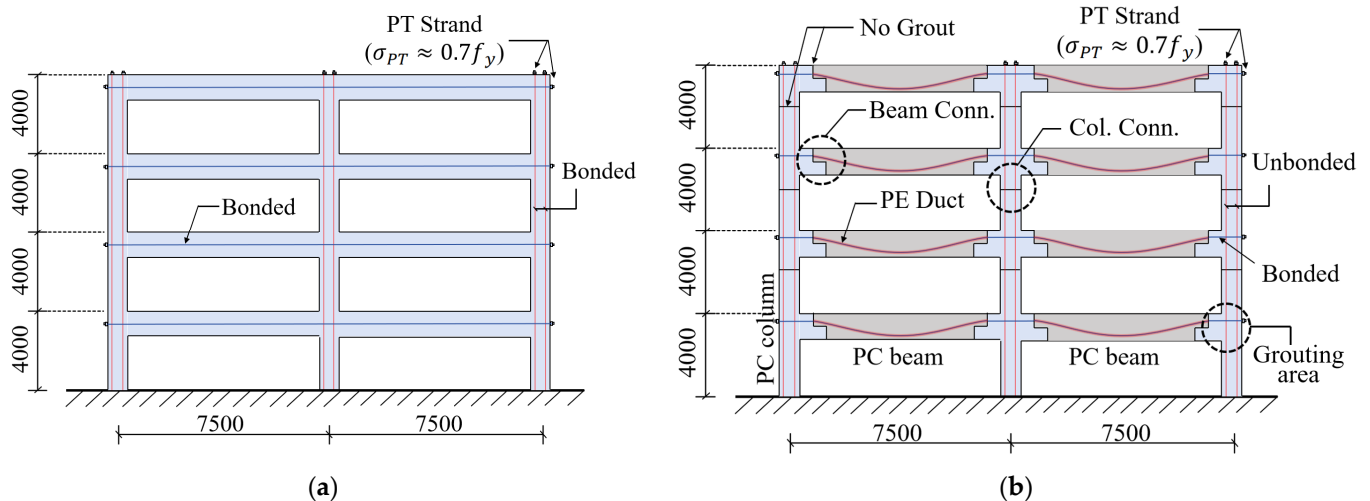


Figure 1. Configuration of frames. (a) Cast-in situ PC frame. (b) PCaPC frame with MT connection.

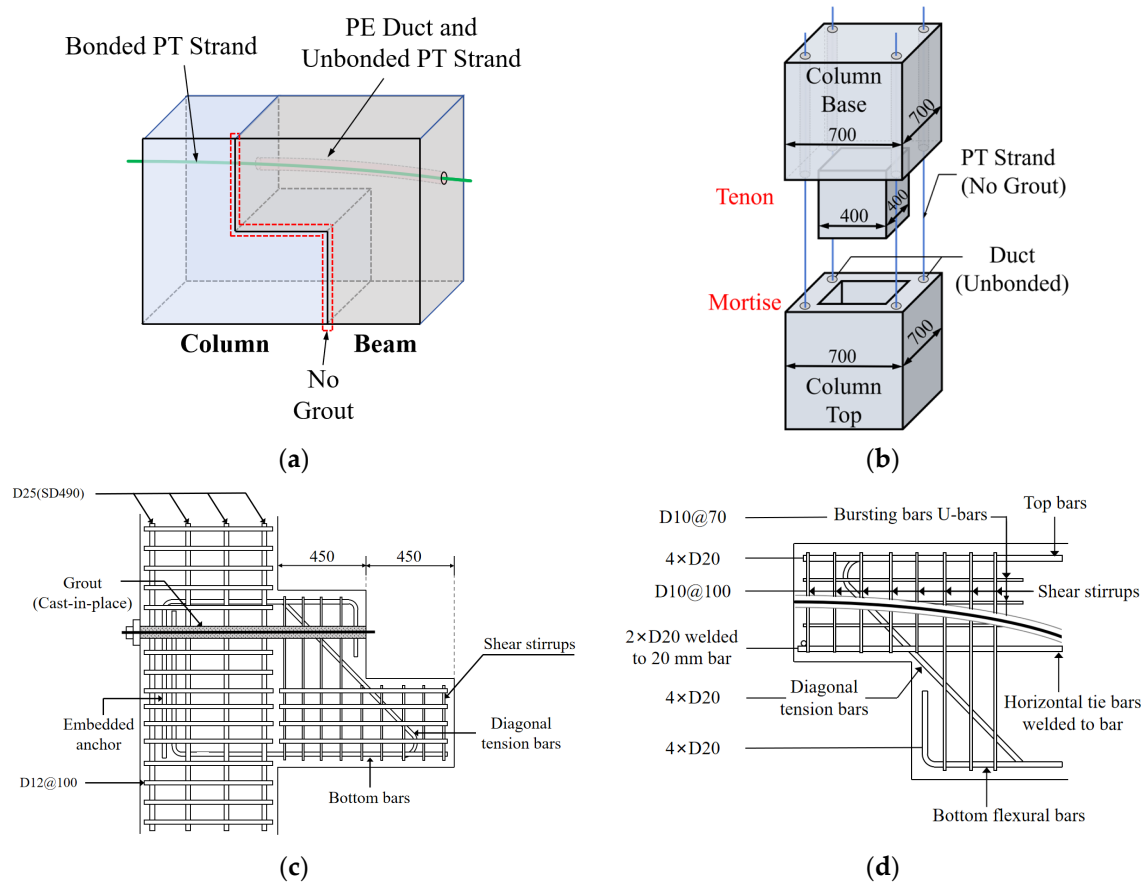


Figure 2. Details of PCaPC frame. (a) Beam-to-column. (b) Column-to-column. (c) Section details of MT column. (d) Section details of MT beam.

Table 1. Designed sections for each frame type.

Frame Type	Precast Elements	Size		Construction		Tendon		
		Section (mm ²)	Beam Length/ Column Height (mm)	PC Type	Grout	PT Strand	Longitudinal	Stirrup
PCaPC	Beam	400 × 900	5900 (Top) 5000 (Bottom)	Partially unbonded	None	Ø12.7	D20	D10@100
	Column	1st Fl. 700 × 700	6000	Unbonded	Reserved hole	Ø12.7	D25	D12@100
		2nd Fl. 700 × 700	4000					
		3rd Fl. 700 × 700	4000					
	4th Fl.	700 × 700	2000					
Cast-in situ PC	Beam	400 × 900	7500	Bonded	Whole area	Ø12.7	D20	D10@100
	Column	700 × 700	4000				D25	D12@100

Table 2. Material parameters of concrete.

Part of Use	Yield Strength (MPa)	Tensile Strength (MPa)	Young's Modulus (GPa)	Poisson's Ratio
Precast	40	6	30	0.2
Cast in situ				

Table 3. Material parameters of tendon.

Part of Use	Diameter	Section (mm ²)	Yield Strength (kN)	Tensile Strength (kN)	Elastic Modulus (GPa)	Poisson's Ratio	Linear Expansion Coefficient	Prestressing Force (kN)
PT tendon	SWPR7BL-Ø12.7	98.7	156	183	195	0.3	1.2×10^{-5}	$0.7f_y = 109.2$
Longitudinal reinforcement	SD490-D10	78.5	490	620	200	0.3	1.2×10^{-5}	-
	SD490-D12	113.1	490	620	200	0.3	1.2×10^{-5}	-
Stirrup	SD490-D20	314.2	490	620	200	0.3	1.2×10^{-5}	-
	SD490-D25	490.9	490	620	200	0.3	1.2×10^{-5}	-

2.2. Construction Method

The connection is considered a key structural performance indicator. The functional success of a precast structure depends largely on the configuration and properties of its inter-element connections. However, to reduce costs, precast designers prefer to control the complicated aspects of the connector at the factory, reducing site operations to simple activities such as dowelling, bolting, and welding.

Based on user-oriented design, a structural design not only needs to safely resist all applied loads and efficiently transfer them to the foundation through the structural elements, it also needs to consider the building's resilience performance, reducing non-elastic damage during earthquakes and maintaining the building's functional integrity. The fabrication and material costs increase with enhancements in connection capacity. Various construction procedures and complex connections are the main factors restricting the popularization of prefabricated structures.

The construction method for the PCaPC frame with MT connections is shown in Figure 3. Compared to most precast frames, the differences lie in the installation methods and the grouting areas. The construction site reduces wet operations such as making formwork and tying rebars. Reserved holes in prefabricated beam and column components allow for the insertion of tenons of adjacent beams into the mortises of another using lifting equipment, followed by tensioning and anchoring. There is no need for bolt installation and energy dissipation devices. Hinge-relocation mechanisms during earthquakes are

achieved through unbonded prestressed strands and the MT configurations in beams. The tensile stress of unbonded prestressed rebars and the self-weight of the superstructure ensure structural stability.

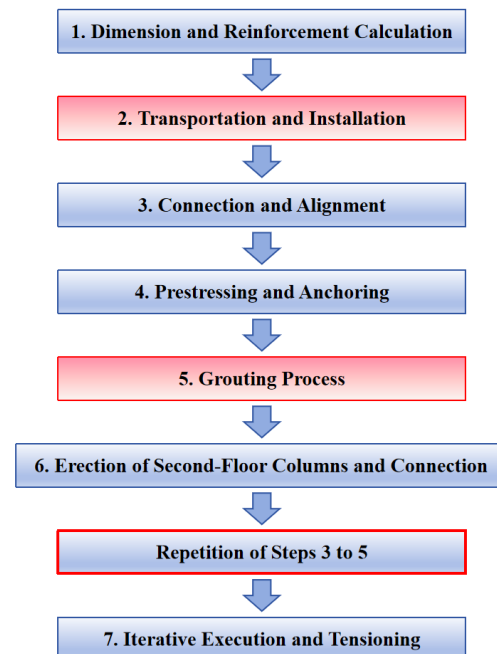


Figure 3. PCaPC with MT connection construction method.

Existing precast frame structures typically require cast-in situ operations at joints or beam ends to connect and secure the precast components. However, MT connections do not require grouting or other cast-in situ operations at the joints. In the structure, grouting is only needed in the reserved holes at the bonded sections of some unbonded PC beams. This simplified construction method reduces the dependence on skilled labor.

2.3. Construction Efficiency and Prefabrication Rate

One aspect of the hindrance of prefabrication is the limited repeatability of prefabricated components. The lack of repetition of components will affect factory productivity and the installation speed. This limitation creates more difficulties in the adoption of prefabrication in the construction industry. Furthermore, some components require replacement after an earthquake, thereby incurring higher construction costs compared to cast-in situ structures. Another hindrance to the adoption of prefabricated construction is the lack of skilled workforces, as it differs from traditional construction. This is due to the lack of experience and knowledge about the design, logistics, and installation of prefabricated components. Therefore, it is necessary to make changes to on-site construction by simplifying the design ahead of improving efficiency levels during the construction phase.

In respect of construction costs, pivotal factors encompass the prefabrication rate, the assembly rate, the building type, the scale, and the structural system of a project, as detailed in Table 4 [38,39]. In China, the assembly rates for PCa construction typically range between 20% and 50%, with cast-in situ methods still prevalent for beam–column connections during the construction process. Furthermore, as assembly rates increase, incremental costs rise, impeding the progress of fully PCa buildings. While the current cost of PCa construction exceeds that of cast-in situ concrete structures, its potential for cost improvement is conceivable. Elevating the repetition rate of PCa components and optimizing component connection designs, particularly streamlining construction processes, emerges as a main strategy for cost reduction.

Table 4. Ratio of PCa construction cost increments in China.

Project Type (City)	Cast-in Situ Cost (JPY/m ²)	PCa Cost (JPY/m ²)	Cost Increase Ratio	Construction Method
Residential (Shanghai)	40,000	56,000	40%	PCa frame–shear wall
Apartment (Nanjing)	34,200	39,000	14%	PCa frame
Apartment (Shenyang)	44,000	50,000	14%	PCa shear wall
		110,000	150%	PCa frame
Residential (Beijing)	40,000	50,000	25%	PCa shear wall
Public rental housing (Shenzhen)	44,000	48,000	9%	PCa shear wall
Residential (Harbin)	40,000	44,000	10%	PCa shear wall
Commodity housing (Changsha)	30,000	34,000	13%	PCa shear wall
Residential (Hefei)	36,000	40,000	11%	PCa shear wall
Average value	38,520	45,120	17%	-

Note. Data from Ministry of Housing and Urban–Rural Development of the People’s Republic of China (MOHURD).

3. Deformation Mechanism

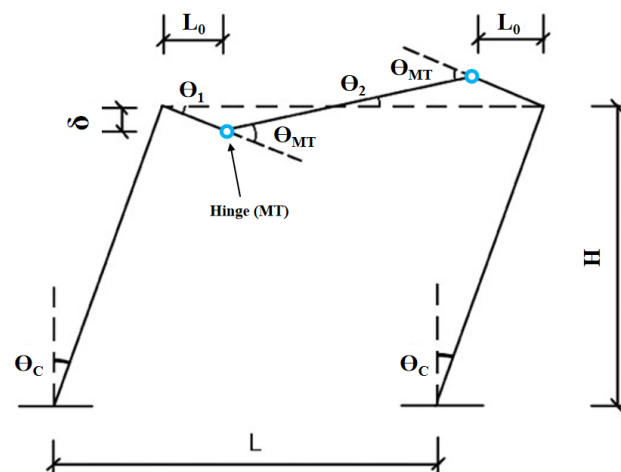
3.1. Hinge-Relocation System

The MT connection changes the deformation mechanism of frame structures. It rotates to dissipate the seismic energy of structures under earthquake action, which greatly delays the formation of the column hinges and improves the reparability of the frame system.

When the hinge system begins to rotate, the beam and the internal unbonded pre-stressed tendons experience slippage, forming lateral displacements during an earthquake. The connection is located away from the joint core area, keeping the columns and joints in the linear elastic phase, as shown in Figure 4. The relationship between the story drift (θ_C) and the hinge rotation angle (θ_{MT}) can be expressed as follows:

$$\theta_{MT} = \theta_1 + \theta_2 = \theta_C \left(1 + \frac{2L_0}{L - 2L_0} \right) = \frac{L}{L - 2L_0} \theta_C \quad (1)$$

where L = the span of the beam, L_0 = the location of MT connection, H = the height of the column, and δ = the vertical displacement of the frame beam.

**Figure 4.** Yield mechanism of the frame.

A simplified deformation model for the MT connection under a bending moment M is shown in Figure 5. The calculation of rotational stiffness is as follows:

$$K_{MT} = \frac{M}{\theta_{MT}} = \frac{(L - 2L_0) \cdot M}{L \cdot \theta_C} \quad (2)$$

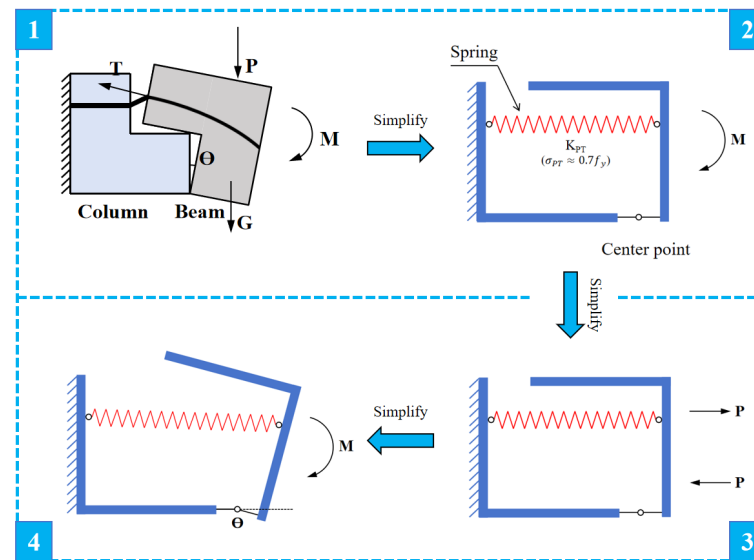


Figure 5. Simplified model of deformation.

3.2. Kinematic State

When the structure is subjected to seismic forces, the seismic waves input into the structure can cause corresponding openings and closings at the connection. As a result, each precast beam and column section can experience slight rotations in a certain direction, creating effects similar to an elastic hinge system. During the seismic process, the MT connection undergoes three stages in response to the variation in mixed seismic waves:

- **Closing Stage:** In the initial phase of an earthquake, the seismic wave amplitude is low, and the seismic damage is weak. The connections of the prefabricated beam and column remain closed, the rotation of the hinges is nearly zero, and the structure has a small effect. This stage is the linear elastic phase. Seismic stresses are small, and the connections remain closed.
- **Hinge-Relocation Stage:** When the amplitude and seismic effects of the mixed seismic waves reach a certain threshold, small openings and closures occur at the connection, forming an elastic hinge system. The seismic action causes the hinge to undergo slight instantaneous rotation, increasing the structure's horizontal displacement and reducing its overall stiffness. Consequently, the instantaneous stress caused by the earthquake is reduced, protecting vulnerable structural nodes from immediate damage and achieving the goal of seismic mitigation. As the mixed seismic waves change, multiple hinge systems undergo varying degrees of rotation, causing continuous changes in the structure's stiffness.
- **Self-Centering Stage:** As the seismic process gradually concludes, seismic action weakens and the energy of seismic waves diminishes. When the amplitude of the seismic waves decreases to a critical value, instantaneous closure occurs at the connection, constrained by the tensile stress of prestressed tendons and the compressive stress from the self-weight of the upper structural elements. The components return to their original positions.

3.3. Failure Mode

Conventional PCaPC frame structures often exhibit a range of failure modes, including tension, compression, and torsion, which add complexity to the structural response. In contrast, the connection design featuring mortises and tenons in a PCaPC structure limits the failure mechanisms primarily to compression. This enhancement of the load-bearing capacity of compression, coupled with the geometric characteristics of MT connections, prevents connections from succumbing to torsional and tensile failures. Specific defor-

mation and hinge-relocation characteristics cause joints to have rigid properties. At the beginning of rotation, the MT connection opens with a bending moment of zero. As the rotation angle gradually increases, the mortise and tenon compress each other tightly and maintain the elastic compression state. With repeated compressive deformation, the edge of the joint yields, as shown in Figure 6b. Moreover, the joint is in the critical state of elastic deformation and elastic–plastic deformation. The failure state of the beam–column connection is shown in Figure 6c. Similarly, the states under negative loading are shown in Figure 7. In addition, an image diagram of the deformation of the column connection is shown in Figure 8.

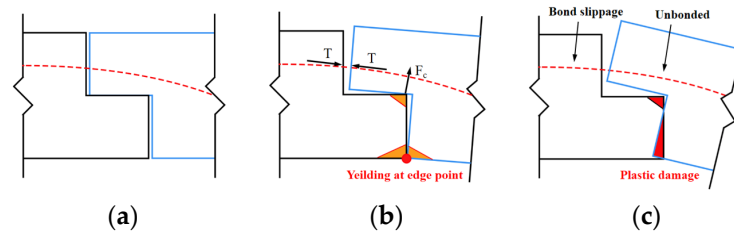


Figure 6. Kinematic states under positive loading. (a) Elastic compression. (b) Plastic compression. (c) Failure state.

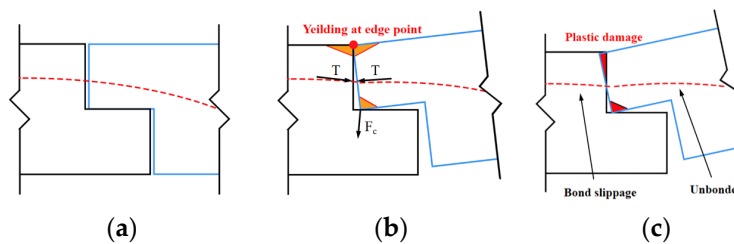


Figure 7. Kinematic states under negative loading. (a) Elastic compression. (b) Plastic compression. (c) Failure state.

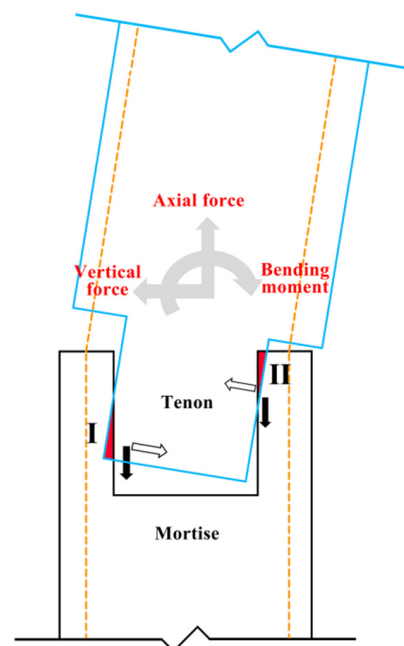


Figure 8. Deformation of column. Areas I and II entering plastic compression state.

4. Finite Element Simulation

In order to construct the seismic response model for the PCaPC frame with MT connections, this paper validates the deformation mechanism of the MT connection through finite element simulation analysis and discusses the load–deformation relationships of beams and columns separately. In this study, the software ABAQUS (2022) was used in the numerical analysis because it can simulate the plasticity and damage of concrete as well as the complex contacts between unbonded prestressed rebars and concrete, which was necessary for this work. The ABAQUS PCaPC model is shown in Figure 9.

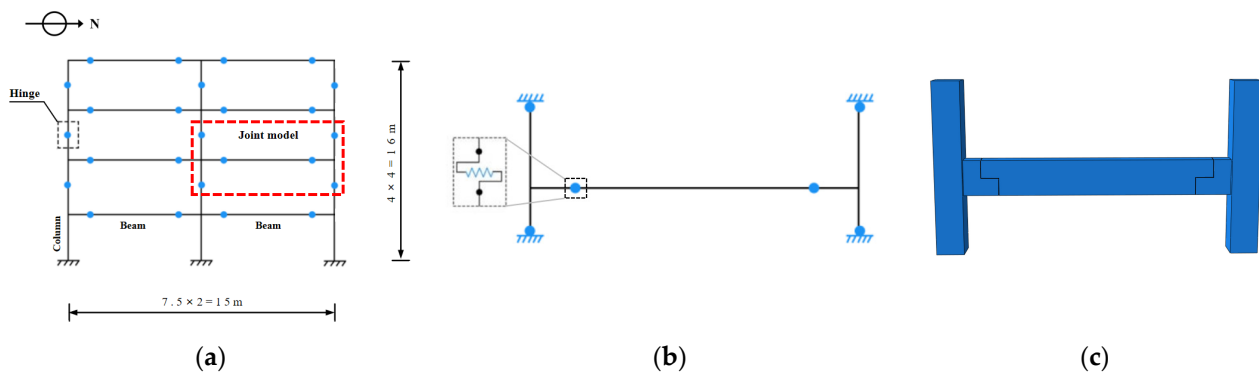


Figure 9. Analytical model of PCaPC frame. (a) Prototype building. (b) Simplified spring joint model. (c) FE joint model.

4.1. Material Model

4.1.1. Concrete Damage Plasticity (CDP) Model

In this study, the Concrete Damage Plasticity (CDP) model was employed to address the complex behavior of concrete, characterized by its non-homogeneous nature. This model, by considering the intricate interplay of plastic deformation and damage accumulation in concrete, provides substantial support for the precise assessment of the performance of prestressed concrete structures. Developed by Lubliner, Lee, and Fenves, the CDP model, serving as a modification of the Drucker–Prager model, accurately simulates compressive and tensile strengths by incorporating crushing and cracking behaviors, as shown in Figure 10. The model’s yield surface in the deviatoric cross section is non-circular, determined by the parameter K_σ , a modification absent in the Drucker–Prager model, with a default value of $2/3$, as per the ABAQUS user’s manual. The material attributes of prestressed tendons are derived from the *PCI Connections Manual*. The material parameters are listed in Table 3, and the size of model is shown in Table 5.

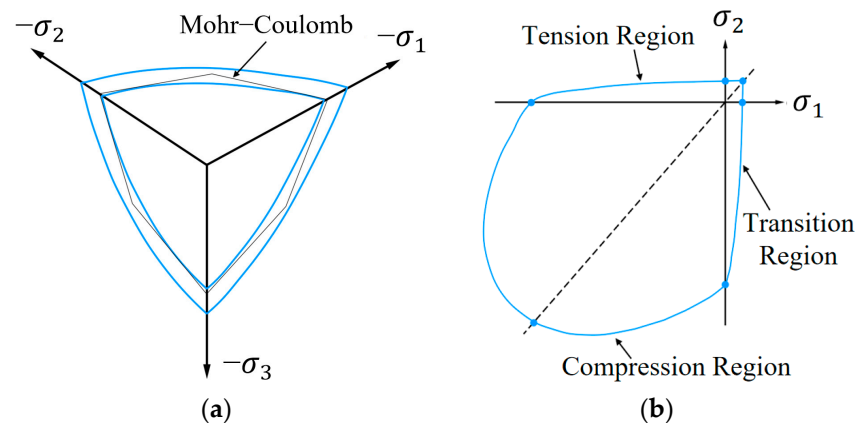


Figure 10. The yield surfaces in the deviatoric plane and the plane stress. (a) The octahedral plane. (b) The plane stress space.

Table 5. Material parameters of FE model.

Material	Param.	Value	Definition	Denotation
Concrete	ϵ	0.1	Flow potential eccentricity	ABAQUS [40]
	φ	38 (rad)	Dilation angle	
	σ_{b0}/σ_{c0}	1.16	Ratio of biaxial to uniaxial compressive	Lubliner et al. [41,42]
	Kc	0.7	Second stress invariant	
	μ	0	Viscosity	ABAQUS [40]
	d	2.85×10^{-9} (t/mm ³)	Density	
	E0	30 (GPa)	Young's modulus	ACI 318 M–11 [43]
	V	0.2	Poisson's ratio	
Prestressed tendons	d	7.8×10^{-9} (t/mm ³)	Density	PCI manual 8–3 [44]
	Es	210 (GPa)	Young's modulus	
	V	0.3	Poisson's ratio	
	α	1.2×10^{-5}	Linear expansion coefficient	

4.1.2. Compressive Behavior of Concrete

In examining the compressive behavior of concrete within the realm of civil engineering, it is imperative to discern distinct phases within the stress–strain curve, as shown in Figure 11 and characterized by Equations (3)–(5) based on [45]. The initial stage characterizes a linear elastic response, indicative of the material's capacity for elastic deformation under compressive loading. Transitioning to the subsequent phase, marked by yielding, reveals non-linear behavior as plastic deformation initiates. Finally, the post-peak region manifests a gradual stress reduction despite increasing strain, signifying the internal damage evolution leading to concrete's ultimate failure under compressive stress.

$$\sigma_c = E_0 \epsilon_{c1} \quad (3)$$

$$\sigma_c^2 = \frac{E_0 \frac{\epsilon_c}{\sigma_{cu}} - \left(\frac{\epsilon_c}{\epsilon_{c2}}\right)^2}{1 + \left(E_0 \frac{\epsilon_c}{\sigma_{cu}} - 2\right) \frac{\epsilon_c}{\epsilon_{c2}}} \sigma_{cu} \quad (4)$$

$$\sigma_c^3 = \sigma_{cu} + (\sigma_{c0} - \sigma_{cu}) \exp \left[0.25 \left(1 - \frac{0.016 - \epsilon_{c2}}{\epsilon - \epsilon_{c2}} \right) \right] \quad (5)$$

where σ_c = concrete compressive stress, σ_{c0} = concrete crushing stress, σ_{cu} = maximum concrete crushing stress, ϵ_c = concrete compressive strain, ϵ_{c1} = concrete crushing strain, ϵ_{c2} = maximum concrete crushing strain, and E_0 = Young's modulus.

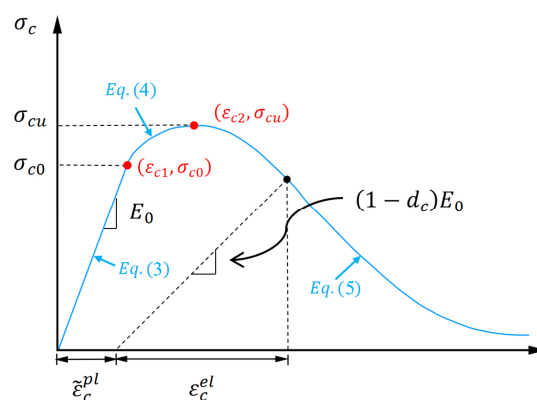


Figure 11. The compressive stress–strain curve.

4.1.3. Tensile Behavior of Concrete

Concrete is inherently strong in compression, but its performance under tensile loading is characterized by a brittle nature and susceptibility to cracking. The stress–strain curve in tension typically exhibits an initial linear elastic region, followed by the onset of non-linearity as microcracks initiate and propagate. The post-cracking behavior, often described as the softening or descending branch, signifies a reduction in stiffness as the cracks evolve and propagate further. The uniaxial tension behavior of concrete is shown in Figure 12 and characterized by Equations (6) and (7) based on [46,47].

$$\sigma_t = E_0 \varepsilon_t \quad (6)$$

$$\sigma_t = \sigma_{t0} \left(\frac{\varepsilon_{t0}}{\varepsilon_t} \right)^{0.4} \quad (7)$$

where σ_t = concrete tensile stress, σ_{t0} = concrete crushing stress, ε_t = concrete tensile strain, ε_{t0} = concrete crushing strain, and E_0 = Young's modulus.

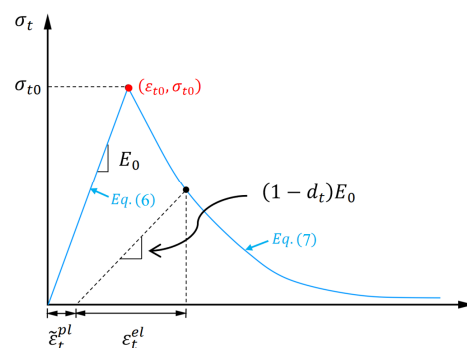


Figure 12. The tensile stress–strain curve.

4.1.4. Modeling of Tendons Materials

The stress–strain relationship proposed by Menegotto and Pinto was used for modeling the prestressing tendon, as shown in Figure 13 and characterized by Equations (8) and (9) based on [48]. The tangent modulus was determined by differentiating the stress–strain equation.

$$\sigma_s = \begin{cases} E_S \varepsilon_S & , \varepsilon_S \leq \varepsilon'_y \\ (1.91 - 2B)f_y + (0.02 + B)E_S \varepsilon_S, & \varepsilon_S > \varepsilon'_y \end{cases} \quad (8)$$

$$f'_y = (0.93 - 2B)f_y, \varepsilon'_y = \frac{f'_y}{E_S}, B = \frac{1}{\rho} \left(\frac{f_t}{f_y} \right)^2 \quad (9)$$

where σ_s = embedded bar stress, ε_S = embedded bar strain, E_S = elastic modulus, f_y = embedded bar yielding strength, f'_y = bare bar yielding strength, ε'_y = embedded bar yielding strain, ρ = reinforcement ratio, and f_t = concrete tensile strength.

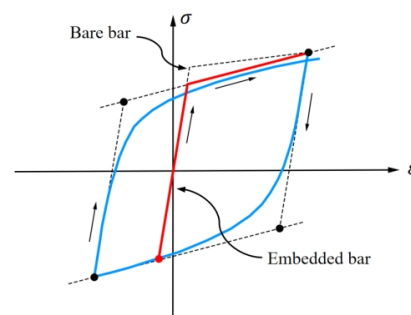


Figure 13. The idealized stress–strain curve for reinforcing rebars.

4.2. Loading Protocol

Cyclic tests were conducted separately on PCaPC and cast-in situ PC models. Gravity loads were applied to the entire model throughout the simulation. After establishing reference points RP1 and RP2, shown in Figure 14a, the coupling method was applied to constrain each reference point with the respective column top surface. This approach allows for controlled transmission of both force and displacement between the reference points and the surfaces. Horizontal loads were applied to reference points RP1 and RP2 at the tops of the two columns, with displacement as the variable, as delineated in Figure 14c.

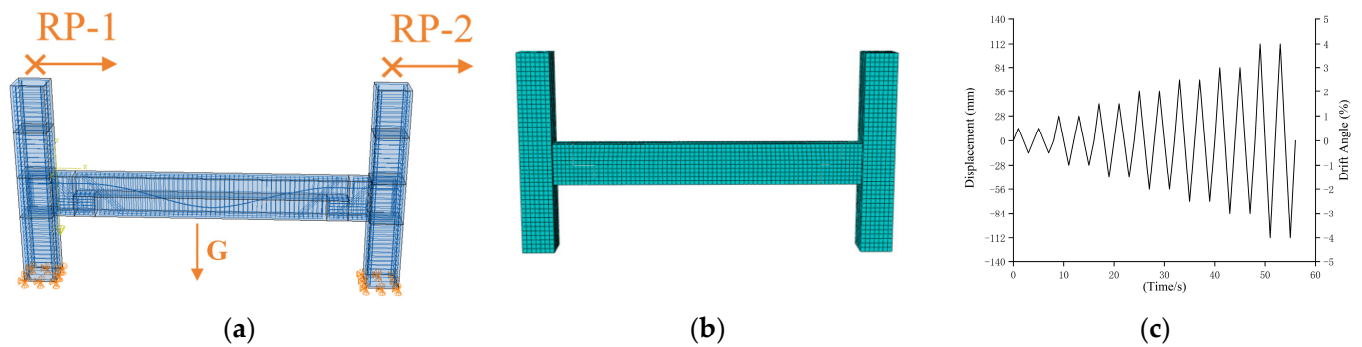


Figure 14. FE model of PCaPC joint. (a) Boundary condition. (b) Mesh model. (c) Loading protocol.

Prefabricated beams were constructed with unbonded prestressed concrete, ensuring free rotation of the beams when subjected to horizontal stresses. The coupling method was employed to constrain prestressed tendons and concrete nodes at the same positions in the beam's height and width directions, thereby releasing degrees of freedom along the length of the beam. The finite element representation of the concrete and rebar elements, integral to understanding their interaction and behavior under stress, is depicted in Figure 15. The contact types between components are as follows: tangential behavior adopts a rough friction formula, while normal behavior uses hard contact, allowing separation after contact.

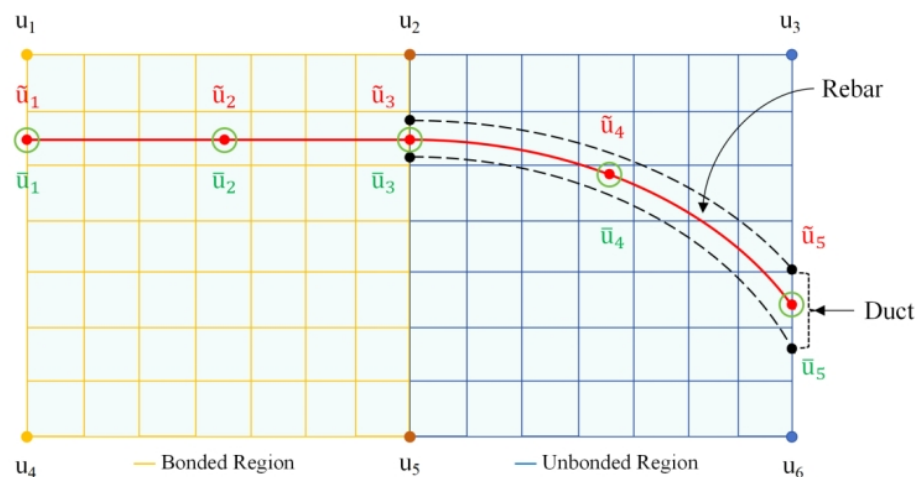


Figure 15. FE representation of concrete and tendon.

4.3. Analysis Results of Stress Map

Figure 16 shows the principal stress distribution for the cast-in situ PC model and the PCaPC model when the inter-story drift angle reaches 0.04 rad. It can be seen that, in the cyclic loading simulation, due to bending failure occurring at the beam ends, the cast-in situ PC frame exhibits stress concentration at the joints. This leads to a gradual increase in inelastic damage and slight bending deformation of the columns at these joints. In contrast,

for the PCaPC frame, the stress distribution is more uniform, indicating that a portion of the tensile force is borne by the unbonded prestressed tendons, delaying the development of concrete deformation and plastic damage. In the PCaPC frame, the high-stress areas mainly appear at one-third of the span and the precast beam–column connections. This is because the MT connections need to withstand and transfer complex seismic forces and deformations. The high-stress areas are influenced by the distribution of internal forces and the complex interactions at the connections, with these effects being more pronounced at one-third of the span rather than at the mid-span.

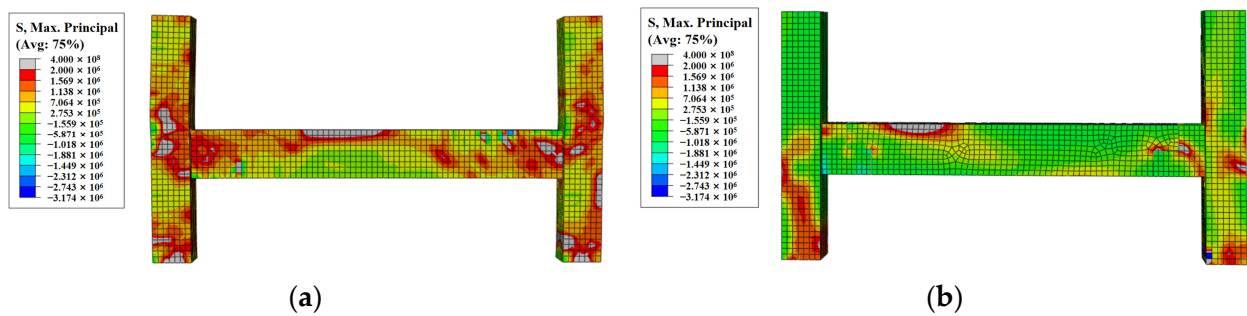


Figure 16. Principal stress distribution at 4% peak drift. (a) Cast-in situ PC. (b) PCaPC with MT connections.

Under 4% peak drift, the Mises stress distributions of the cast-in situ PC and PCaPC with MT connection structures exhibit distinct characteristics, as shown in Figure 17. For the cast-in situ PC structure, stress is primarily concentrated at the beam–column joints and beam ends. Particularly in the connection region, high localized stress poses a risk of plastic deformation and yielding. Furthermore, due to the combined effects of bending moments and shear forces, the stress distribution at the beam–column joints is uneven, which may lead to localized damage.

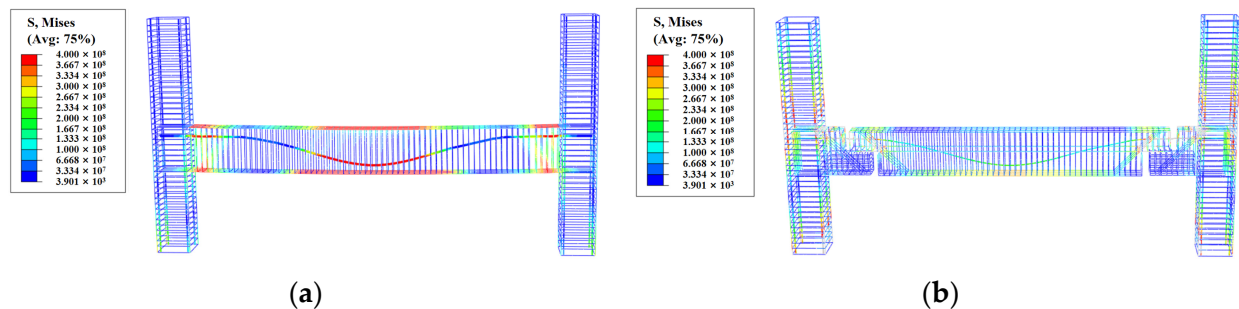


Figure 17. Mises stress distribution of tendons at 4% peak drift. (a) Cast-in situ PC. (b) PCaPC with MT connections.

In contrast, the PCaPC structure with unbonded prestressing tendons shows a different stress distribution. The unbonded tendons are free to slide along the length of the beam, allowing the stress to be distributed more uniformly across a larger area and reducing the likelihood of localized stress concentrations. Although stress concentrations still occur at the MT connections, the ability of the unbonded tendons to move freely along the beam reduces stress accumulation in the middle region, resulting in a more even overall stress distribution. This uniformity helps mitigate localized damage under large deformations, and the unbonded prestressing system allows the structure to return to its near-original state after unloading.

4.4. Comparison of Failure Modes

Figure 18 shows the equivalent plastic strain for both the cast-in situ PC frame and the PCaPC frame, revealing distinct plastic deformation characteristics for each. The results indicate that plastic deformation in the cast-in situ PC frame is primarily concentrated at the joints. This concentration is due to stress concentration and material non-linearity at the joints under cyclic loading, where these areas experience high bending moments and shear forces, resulting in significant plastic deformation.

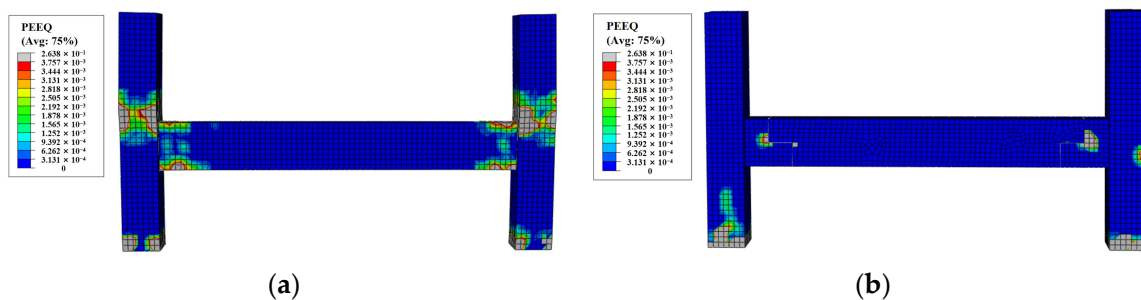


Figure 18. Equivalent plastic strain at 4% peak drift. (a) Cast-in situ PC. (b) PCaPC with MT connections.

In contrast, plastic strain in the PCaPC frame accumulates mainly at the MT connections. During cyclic loading, these MT connections undergo rotation and reset, with the prestressing tendons providing horizontal force restraint that assists in restoring the connections to their original positions. The compression damage progressively accumulates at the MT connections. Indeed, the columns of the PCaPC frame largely remain elastic under cyclic loading.

4.5. Hysteresis Loops

To extract hysteresis characteristics for both beam and column components in the PCaPC and cast-in situ PC frame models, separate simulations were conducted with specific configurations tailored to each component. In the first simulation, the columns were modeled with elastic material properties, while the beams exhibited plastic behavior. Conversely, in the second simulation, the columns were simulated with plastic behavior, while the beams retained elastic properties. These distinct simulation conditions were necessary to capture the different hysteresis characteristics of beams and columns under cyclic loading.

Figures 19 and 20 depict the hysteresis loops and skeleton curves of the cast-in situ PC and PCaPC models, explicitly focusing on beam connection, column connection, and the overall frame. A feature observed during cyclic testing of the PCaPC frame with MT connections is the absence of a descending portion in the hysteresis curve. Unlike the cast-in situ PC frame, the load–displacement curve maintains an upward trajectory even after undergoing multiple loading cycles. This behavior is a testament to the capacity of MT connections to sustain elastic deformation throughout repetitive loading. The columns exhibit elastic behavior without signs of plastic damage, maintaining a continuous linear state in the hysteresis curve. This observation underscores the column’s ability to endure loading cycles while preserving its elastic characteristics.

Figure 21 compares the residual drifts of the cast-in situ PC structure and the PCaPC structure after unloading at 4% drift angle. Due to the columns being within the elastic range, the residual drift in PCaPC is minor, with a maximum drift rate of 0.52%. Compared to the cast-in situ PC frame, the residual drift in the PCaPC frame is reduced by 0.78 times. The reduction in residual drift demonstrates the effectiveness of the MT connection in enhancing the reparability performance of the frame.

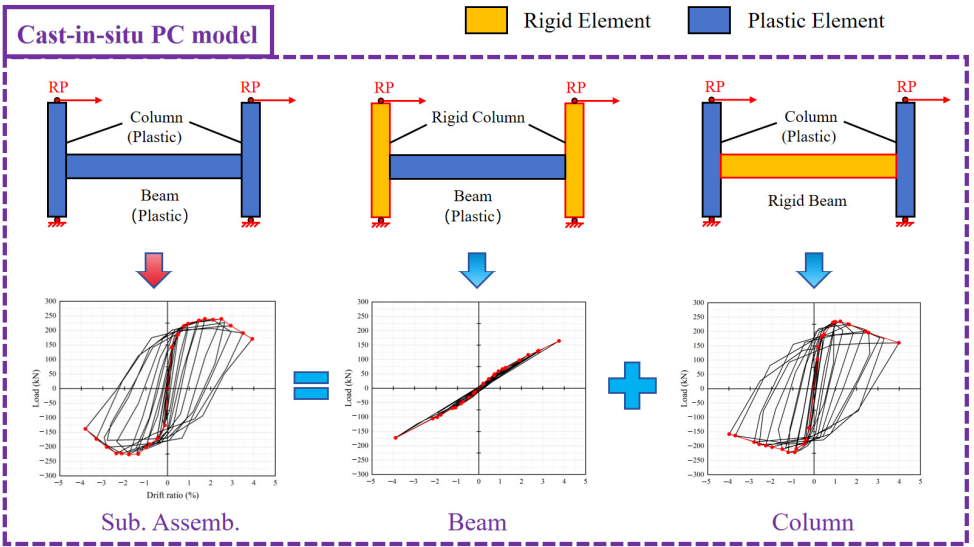


Figure 19. Hysteresis loops of cast-in situ PC with explanatory diagrams.

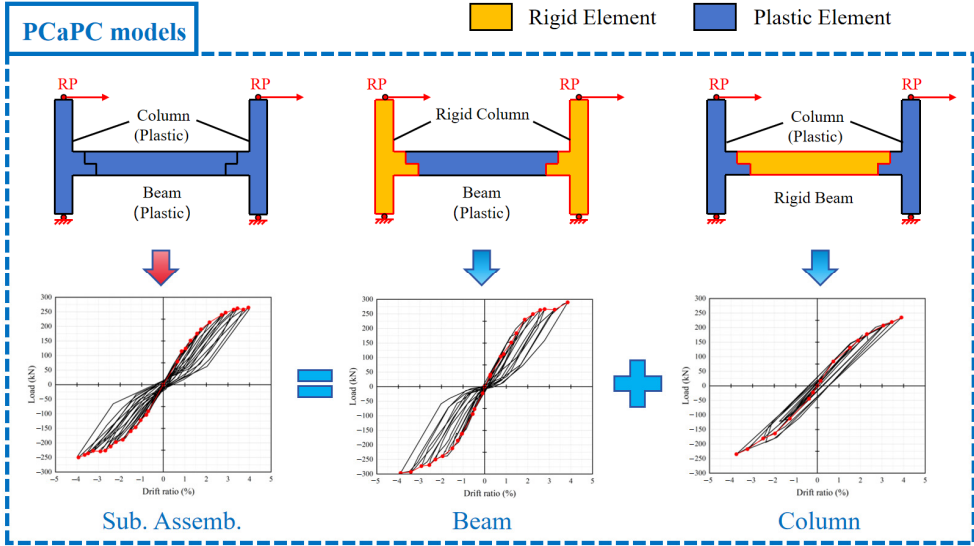


Figure 20. Hysteresis loops of PCaPC with explanatory diagrams.

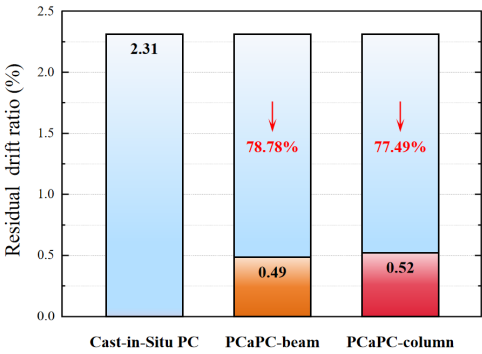


Figure 21. Comparison of residual drift ratios after 4% peak drift.

5. Seismic Response Analysis

5.1. Seismic Response Model

The seismic response analysis method is a fundamental and important technique for structural dynamic analysis. Seismic response analysis can generally be performed using finite element software and programming software, each with its own characteristics. Finite element software, such as ABAQUS (2022), can create complex mortise–tenon geometric models and simulate the plastic damage of non-linear materials like concrete, including cracking and deformation, as well as the complex contact problems in partially unbonded prestressed concrete. However, the computational time cost of finite element software is high, making it challenging to conduct a large number of seismic response analyses and obtain engineering demand parameters (EDPs) in a short period. Due to the extensive calculations involved in seismic response analysis, efficiency is crucial. To make the loss estimation of PCaPC frames and PC frames easier, this paper employed a simple seismic response analysis model.

In developing this model, it was assumed that the simplified spring model can adequately capture the main seismic response characteristics of both PCaPC and PC frames, particularly their hysteresis behavior and variations in structural stiffness under seismic loading. To reduce computational complexity, the spring model simplifies the geometry and contact aspects of the connections while still effectively simulating the critical seismic response of these joints. Although the geometric details and contact issues were simplified, the hysteresis characteristics were derived from prior finite element analyses using ABAQUS. These analyses established detailed mortise–tenon geometric models and simulated the non-linear plastic behavior of concrete. The hysteresis data obtained from these FEA simulations were then incorporated into the simplified model, ensuring that the key mechanical responses were accurately represented.

A four-story PCaPC frame structure, assumed to be built in Sendai, Japan, was selected for the case study in this paper. Two seismic response models were created using finite element analysis (FEA) software (MATLAB 2024): one for a cast-in situ PC frame and the other for a PCaPC frame with MT connections. Both models employ identical material properties and cross sections, as detailed in Table 1 and Figure 1. The PCaPC model utilizes partially unbonded prestressing tendons with prefabricated connections that are not subjected to cast-in situ operations, allowing for separation during an earthquake. In contrast, the cast-in situ PC model employs bonded prestressing tendons. The lower part of Figure 22 illustrates the elevation view of the building in a wireframe model. The building is located on a site classified as high seismic hazard.

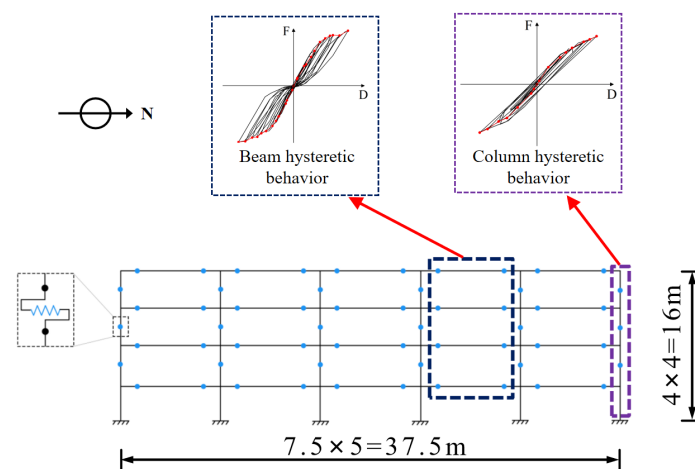


Figure 22. Seismic response model.

The component-end spring model was chosen to simulate the seismic behavior of the MT connection. Hysteresis characteristics were derived from the load–deformation

relationship obtained from previous FEA, and a seismic response analysis model was established using MATLAB software (2024) with the Newmark- β method, as depicted in Figure 22. Subsequently, one-component frame models were developed:

1. Geometric Configuration: The “Materials and Section Properties” and “Structural Parameters” of the frame model were defined, detailed in Tables 1–3, encompassing dimensions of beam and column sections, story height, span, Young’s modulus, and other relevant parameters.
2. Consideration of MT Connection: Modeling the MT connection required simultaneous consideration of hysteresis and restoring force characteristics. The PCaPC frame model was segmented into two components: the Beam model and the Column model. The Beam model’s hysteresis characteristics utilized the Origin-Oriented Model, whereas the Column model employed an elastic model. Hysteresis characteristics were computed based on hysteresis curves obtained from previous cyclic loading simulations, as illustrated in Figure 22.
3. Development of Spring Model: The component-end spring model for the PCaPC frame was constructed, incorporating input parameters such as the following:
 - f_c : Cracking Strength;
 - f_y : Yield Strength;
 - a_y : Ratio of Secant Stiffness to Elastic Stiffness at Yield Point;
 - a_u : Ratio of Post-Yield Stiffness to Elastic Stiffness.

The proposed framework for the seismic response model is shown in Figure 23. Employing Japan Meteorological Agency (JMA)-sourced ground motion records, our analysis conducted non-linear dynamic response evaluations to accurately quantify structural responses like inter-story drift ratios and peak floor accelerations under varied seismic intensities. This was achieved by employing the load–deformation relationships derived from finite element analysis using ABAQUS, which facilitated a detailed examination of the hysteresis characteristics. Subsequently, these characteristics were integrated into a simplified spring structural model to make seismic response analysis easier for conducting non-linear dynamic response simulations in Matlab.

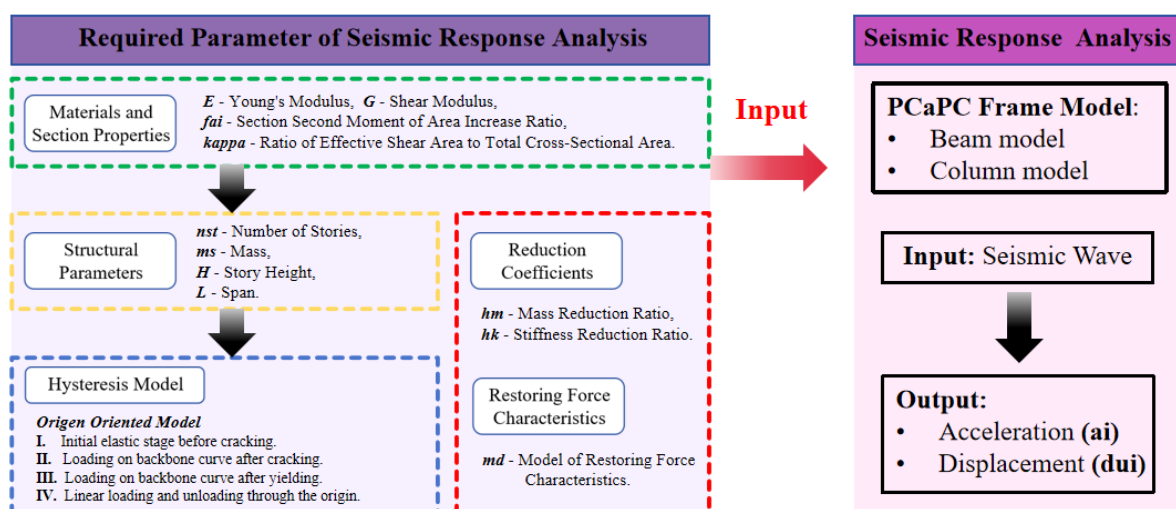


Figure 23. Proposed framework for seismic response analysis.

5.2. Ground Motion Selection

A selection of NS-direction strong-motion observation data were gathered from the Japan Meteorological Agency (JMA), as shown in Table 6. Taking PGV as the Intensity Measure (IM), the above ground motion records were input after amplitude modulation to study the seismic performance of cast-in situ PC and PCaPC frames.

Table 6. Ground motions selected for case study.

Seismic Hazard	Earthquake	Mw	Depth (km)	Station	Distance (km)	Soil Type
50% in 50 years (PGV = 18.6 cm/s)	Hokkaido Eastern Iburi 21 February 2019	5.8	33	Kanuma Shin-Kotoni	17.3 67.1	Level 4 Level 4
	Osaka Northern 18 June 2018	6.1	13	Chayamachi Mukaijima	18.7 16.3	Level 4 Level 4
	Near Awaji Island 13 April 2013	6.3	11	Kojidani Nakada	11.8 5.1	Level 4 Level 4
	Ibaraki Northern 28 December 2016	6.3	15	Kakuuchi Kanamachi	55.4 39.1	Level 3 Level 4
	Noto Peninsula Offshore 5 May 2023	6.5	12	Misakacho Monzencho	11 55.1	Level 3 Level 2
				Hashide		
	Nagano Northern 22 November 2014	6.7	5	Hakoshimizu Otemachi	27.4 55.7	Level 4 Level 4
10% in 50 years (PGV = 36.5 cm/s)	Yamagata-Oki 18 June 2019	6.7	14	Fuyasu Babacho	11.5 33.1	Level 4 Level 4
	Niigata Chuetsu 23 October 2004	6.8	13	Kawaguchi Chitosecho	2.8 21	Level 4 Level 4
	Fukuoka Northwestern Offshore 20 March 2005	7.0	9	Maizuru Tsufukumotocho	26.1 57.1	Level 4 Level 4
				Ofunatocho	27.5	Level 2
	Miyagi Offshore 26 May 2003	7.1	72	Izumicho	53.4	Level 3
5% in 50 years (PGV = 44.2 cm/s)	Tottori Western 06 October 2000	7.3	9	Higashihonmachi Nishigochi	31.4 45.3	Level 4 Level 2
	Noto Peninsula 01 January 2024	7.6	16	Fugeshimachi Misakimachi	35.2 9.3	Level 4 Level 3

In this study, multiple strong-motion records were employed in the non-linear time history response analysis to minimize the variation in response due to strong-motion characteristics. The dataset spans from the year 2000 to 2024. To represent three distinct seismic hazard levels, corresponding to probabilities of exceeding 50%, 10%, and 5% within 50 years, the records were scaled using peak ground velocity (PGV). The PGV values for each hazard level were obtained from the Japan Seismic Hazard Information Station (J-SHIS), based on the location of the prototype building at Tohoku University's Aobayama Campus in Sendai, Japan. Table 6 presents four representative seismic waves for each hazard level, scaled according to the PGV values, that were used to perform the seismic response analysis.

5.3. Structural Response

This analysis scrutinized a modular frame structure utilizing MT connections with unbonded PCaPC, as described in Section 2, against a cast-in situ PC frame with bonded tendons. For future calculations of Damage Measures (DMs), the selected engineering demand parameters (EDPs) are the inter-story drift ratio and the absolute floor acceleration, as shown in Table 7. According to the FEMA-P58 methodology [49], three categories of building components are delineated: structural components, non-structural components, and building contents. Each category is influenced by specific EDPs that help in assessing building performance and estimating repair costs. For instance, non-structural components are divided into displacement-sensitive and acceleration-sensitive groups based on their susceptibility to seismic impacts.

Table 7. Performance group of components.

Type	Components	FEMA P58 ID	EDP
S	MT connection	-	du _i
S	Beams	B1031.011b	du _i
S	Columns	B1031.021b	du _i
N	Curtain walls	B1035.021	du _i
N	Prefabricated stair	B1035.031	du _i
N	Suspended ceiling	B2022.001	a _i
N	Independent pendant lighting	C2011.011b	a _i
N	Cold or hot potable	C3032.003a	a _i
N	Sanitary waste piping	C3034.001	a _i
N	HVAC	D2021.011a	a _i
C	Modular office work stations	D2031.011b	a _i
C	Unsecured fragile objects on shelves	D3041.001a	a _i
C	Electronic equipment on wall mount brackets	E2022.001	a _i
C	Desktop electronics	E2022.010	a _i
C	Bookcase	E2022.021	a _i

S = structural component, N = non-structural component, C = content, d_{ui} = inter-story drift ratio at the ith story, a_i = absolute floor acceleration at the ith floor.

The key findings of this analysis are detailed in Table 8, which presents the mean values of the engineering demand parameters (EDPs). Notably, these EDPs encompass “du_i,” the inter-story drift ratio at the ith story, and “a_i,” the absolute floor acceleration at the ith floor. In this research, even though the cast-in situ PC and PCaPC structures utilized identical materials and shared the same dimensions, including beam and column sizes, the cast-in situ PC structure demonstrated greater rigidity. This increased rigidity is reflected in these EDPs, leading to higher floor accelerations under seismic loading when compared to the PCaPC structure.

Table 8. Engineering demand parameters.

EDP	Hazard Level					
	50% in 50 Yrs.		10% in 50 Yrs.		5% in 50 Yrs.	
	Cast-in Situ PC	PCaPC	Cast-in Situ PC	PCaPC	Cast-in Situ PC	PCaPC
du1 [%]	0.46	0.37	1.03	0.64	1.56	1.27
du2 [%]	0.59	0.31	1.13	0.51	1.81	1.01
du3 [%]	0.53	0.32	1.01	0.52	1.86	1.12
du4 [%]	0.41	0.15	0.97	0.26	1.66	0.74
a1 [g]	0.68	0.44	0.79	0.73	1.19	0.98
a2 [g]	0.59	0.43	0.56	0.37	1.33	0.91
a3 [g]	0.49	0.28	0.52	0.34	1.19	0.84
a4 [g]	0.29	0.21	0.36	0.24	0.99	0.53

Note: Values in parentheses represent standard deviations.

The median inter-story drift and acceleration of PCaPC and cast-in situ PC frames were compared under the three hazard levels considered. At the “50% in 50 years” hazard level, the floor accelerations of both frames decreased with height. However, as the intensity of shaking increased to the “5% in 50 years” hazard level, the decrease in floor acceleration with height became less pronounced. This was because, during strong ground motion, the lower floors of the structure may enter the non-linear response stage, reducing stiffness and load-bearing capacity. Consequently, more seismic energy is dissipated in the lower floors, causing the decrease in acceleration with height to be less noticeable. Non-linear response alters the dynamic characteristics of the structure, affecting the propagation path of seismic waves, resulting in a more uniform distribution of floor accelerations.

In the seismic response analysis, the maximum acceleration of the PCaPC frame was 0.98 g, while the maximum acceleration of the cast-in situ PC frame was 1.33 g. This implies that the PCaPC frame experiences lighter damage during an earthquake, mainly concentrated on non-structural components, leading to a shorter recovery time for the building system. Conversely, the cast-in situ PC frame, due to its higher acceleration, may suffer moderate to severe damage, including deformation and cracks in primary structural components, and significant permanent deformation, leading to increased repair costs and time. Overall, the PCaPC frame demonstrates higher safety and economic efficiency under seismic loading. Its lower acceleration effectively reduces damage to structural components, enhancing post-earthquake functionality. Even under the strong earthquake with a “5% in 50 years” hazard level, the stiffness-adjustment mechanism of the PCaPC structure can effectively control deformation and vibrations.

The seismic response analysis results align with the hysteresis characteristics discussed earlier, reflecting their different seismic behaviors. The PCaPC structure’s hysteresis curves exhibit smaller areas with reducing seismic response. Although this characteristic results in smaller hysteresis loop areas, it suggests that the PCaPC structure may be able to maintain smaller residual displacements post-earthquake, thereby enhancing seismic performance. In contrast, the cast-in situ PC structure dissipates seismic energy through larger plastic deformations and hysteresis loop areas, which may lead to greater displacements and higher repair costs.

6. Conclusions

In this paper, a PCaPC frame with hinge-relocated mortise–tendon connections was proposed. The precast components are connected by partially unbonded prestressed tendons, forming a system similar to an elastic hinge. A quasi-static cyclic loading finite element (FE) simulation of the PCaPC frame and the cast-in situ PC frame was conducted on two models to understand the behavior of the PCaPC frame with MT connections. Additionally, the load–deformation relationships were referenced to establish a simple seismic response analysis model. Based on the FE results and seismic response analysis, the following conclusions can be drawn:

1. The PCaPC frame does not require grouting and other complex procedures for connections. Without increasing incremental costs, it enhances the assembly rate of buildings and simplifies the complexity of on-site construction.
2. The yield mode of the PCaPC frame was the compression yield of the tenon edge, and the ultimate mode was the compression failure in the area of the MT connection, which achieved the purpose of damage control. Moreover, the pull stress of the unbonded prestressed rebars combined with the self-weight of the upper structure restores the components to their original position after loading, thus guaranteeing the resilience performance of the MT connections.
3. The finite element simulations reveal that damage to the cast-in situ PC frame is primarily concentrated at the column joints, leading to an increase in residual displacements. In contrast, damage to the PCaPC frame was mainly observed at the MT connections, manifesting as compression failure, with the columns maintaining their elasticity and avoiding noticeable inelastic damage. The overall residual displacements of the PCaPC frame are substantially lower.
4. This study presents a seismic response analysis model that makes the analysis process simple and conducted a seismic response analysis for both PCaPC and cast-in situ PC frames. The results indicate that, under the same seismic hazard levels, the inter-story drift ratio and acceleration ratio of the PCaPC frame are lower than those of the cast-in situ PC frame. This divergence in performance was consistently observed, even under heightened seismic risk conditions, such as those represented by the 5% in 50 years hazard level.

Author Contributions: Conceptualization, H.Z. and N.T.; methodology, H.Z. and N.T.; formal analysis, H.Z. and N.T.; investigation, H.Z.; writing—original draft preparation, H.Z.; writing—review and editing, H.Z. and N.T.; supervision, N.T. All authors have read and agreed to the published version of the manuscript.

Funding: This research received no external funding.

Data Availability Statement: The data presented in this study are available upon request from the corresponding author.

Conflicts of Interest: The authors declare no conflicts of interest.

References

- Bertram, N.; Fuchs, S.; Mischke, J.; Palter, R.; Strube, G.; Woetzel, J. *Modular Construction: From Projects to Products*; McKinsey & Company: New York, NY, USA, 2019; pp. 1–34.
- Lim, J.; Son, C.B.; Kim, S. Scenario-based 4-D dynamic simulation model for in-situ production and yard stock of precast concrete members. *J. Asian Arch. Build. Eng.* **2023**, *22*, 2320–2334. [\[CrossRef\]](#)
- EU. Regulation (EU) No 305/2011 of the European Parliament and of the Council of 9 March 2011. *Off. J. Eur. Communities* **2016**, *269*, 1–15.
- Liu, D.; Li, X.; Chen, J.; Jin, R. Real-time optimization of precast concrete component transportation and storage. *Adv. Civ. Eng.* **2020**, *2020*, 5714910. [\[CrossRef\]](#)
- Xu, Z.; Wang, S.; Wang, E. Integration of BIM and energy consumption modelling for manufacturing prefabricated components: A case study in China. *Adv. Civ. Eng.* **2019**, *2019*, 1609523. [\[CrossRef\]](#)
- Dong, Y.H.; Jaillon, L.; Chu, P.; Poon, C.S. Comparing carbon emissions of precast and cast-in-situ construction methods—A case study of high-rise private building. *Constr. Build. Mater.* **2015**, *99*, 39–53. [\[CrossRef\]](#)
- Hong, J.; Shen, G.Q.; Li, Z.; Zhang, B.; Zhang, W. Barriers to promoting prefabricated construction in China: A cost–benefit analysis. *J. Clean. Prod.* **2018**, *172*, 649–660. [\[CrossRef\]](#)
- Li, X.; Wang, C.; Alashwal, A.; Bora, S. Game analysis on prefabricated building evolution based on dynamic revenue risks in China. *J. Clean. Prod.* **2020**, *267*, 121730. [\[CrossRef\]](#)
- Jeong, J.; Jeong, J. Quantitative methodology of environmental impact and economic assessment under equivalent conditions for prefabricated systems. *J. Build. Eng.* **2023**, *76*, 107104. [\[CrossRef\]](#)
- Gan, X.; Chang, R.; Zuo, J.; Wen, T.; Zillante, G. Barriers to the transition towards off-site construction in China: An Interpretive structural modeling approach. *J. Clean. Prod.* **2018**, *197*, 8–18. [\[CrossRef\]](#)
- Zhou, Z. The Obstacles to Promoting the Modular Building Project: A Tentative Assessment of the Literature. *Technol. Innov. Eng. Res.* **2022**, *6*, 1–6.
- Navaratnam, S.; Ngo, T.; Gunawardena, T.; Henderson, D. Performance review of prefabricated building systems and future research in Australia. *Buildings* **2019**, *9*, 38. [\[CrossRef\]](#)
- Almashaqbeh, M.; El-Rayes, K. Minimising transportation cost of prefabricated modules in modular construction projects. *Eng. Constr. Archit. Manag.* **2022**, *29*, 3847–3867. [\[CrossRef\]](#)
- Jin, H.; Qu, X.; Liu, B.; Liu, C. Examining the success drivers and barriers of modular building projects using qualitative comparative analysis. *Int. J. Constr. Manag.* **2022**, *24*, 601–609. [\[CrossRef\]](#)
- Guaygua, B.; Sánchez-Garrido, A.J.; Yepes, V. A systematic review of seismic-resistant precast concrete buildings. *Structures* **2023**, *58*, 105598. [\[CrossRef\]](#)
- Wang, Y.; Feng, Y.; Huang, D.; Huang, Z.; Chen, Z. Restoring Force Model of an Energy-Dissipation Joint in Hybrid Frames: Simplified Skeleton Curve and Hysteretic Rules. *Adv. Civ. Eng.* **2020**, *2020*, 7806381. [\[CrossRef\]](#)
- Huang, H.; Yuan, Y.; Zhang, W.; Li, M. Seismic behavior of a replaceable artificial controllable plastic hinge for precast concrete beam-column joint. *Eng. Struct.* **2021**, *245*, 112848. [\[CrossRef\]](#)
- Yuan, Y.; Huang, H.; Ye, Y.; Li, M.; Sun, H. Performance coordination design method applied to replaceable artificial controllable plastic hinge for precast concrete beam-column joints. *J. Build. Eng.* **2022**, *47*, 103863. [\[CrossRef\]](#)
- Huang, H.; Li, M.; Yuan, Y.; Bai, H. Experimental research on the seismic performance of precast concrete frame with replaceable artificial controllable plastic hinges. *J. Struct. Eng.* **2023**, *149*, 04022222. [\[CrossRef\]](#)
- Sun, D.; Yang, Y.; Ma, Y.; Xue, Y.; Yu, Y.; Feng, S. Seismic performance of resilient beam-column connection using replaceable stiffener angle steel. *J. Constr. Steel Res.* **2022**, *196*, 107370. [\[CrossRef\]](#)
- Yang, Y.; Gao, S.; Zheng, Y.; Liu, X.; Zhang, W.; Lin, B.Q. Seismic performance of precast column-beam joint with artificial plastic hinge. *J. Build. Eng.* **2023**, *67*, 105942. [\[CrossRef\]](#)
- Zhang, W.X.; Wu, H.; Zhang, J.Y.; Wang, X.; Yi, W.J. Experimental test on progressive collapse resistance of the spatial behavior of integrated precast concrete frame substructures. *China Civ. Eng. J.* **2020**, *53*, 42–56.
- Kang, S.B.; Tan, K.H.; Yang, E.H. Progressive collapse resistance of precast beam–column sub-assemblages with engineered cementitious composites. *Eng. Struct.* **2015**, *98*, 186–200. [\[CrossRef\]](#)

24. Feng, F.F.; Hwang, H.J.; Yi, W.J. Static and dynamic loading tests for precast concrete moment frames under progressive collapse. *Eng. Struct.* **2020**, *213*, 110612. [\[CrossRef\]](#)
25. Negro, P.; Bournas, D.A.; Molina, F.J. Pseudodynamic tests on a full-scale 3-storey precast concrete building: Global response. *Eng. Struct.* **2013**, *57*, 594–608. [\[CrossRef\]](#)
26. Sousa, R.; Batalha, N.; Rodrigues, H. Numerical simulation of beam-to-column connections in precast reinforced concrete buildings using fibre-based frame models. *Eng. Struct.* **2020**, *203*, 109845. [\[CrossRef\]](#)
27. de Lima Araújo, D.; Prado, L.P.; da Silva, E.B.; El Debs, M.K. Temporary beam-to-column connection for precast concrete frame assembly. *Eng. Struct.* **2018**, *171*, 529–544. [\[CrossRef\]](#)
28. Parastesh, H.; Hajirasouliha, I.; Ramezani, R. A new ductile moment-resisting connection for precast concrete frames in seismic regions: An experimental investigation. *Eng. Struct.* **2014**, *70*, 144–157. [\[CrossRef\]](#)
29. Kurosawa, R.; Sakata, H.; Qu, Z.; Suyama, T. Precast prestressed concrete frames for seismically retrofitting existing RC frames. *Eng. Struct.* **2019**, *184*, 345–354. [\[CrossRef\]](#)
30. Jin, K.; Kitayama, K.; Song, S.; Kanemoto, K.O. Shear Capacity of Precast Prestressed Concrete Beam-Column Joint Assembled by Unbonded Tendon. *Proc. Am. Concr. Inst. Struct. J.* **2017**, *114*, 04022222. [\[CrossRef\]](#)
31. Jin, K.; Kitayama, K. Evaluation Method of Skelton Curve for Unbonded PCaPC Beam Member in Exterior Beam-Column Joint Subassembly. *Proc. Jpn. Concr. Inst.* **2019**, *41*, 481–486.
32. Jin, K.; Hao, L.; Kitayama, K. Direct Evaluation Method for Load-Deformation Curve of Precast Prestressed Concrete Frame with Different Tendon Forces. *Bull. Earthq. Eng.* **2021**, *19*, 3597–3626. [\[CrossRef\]](#)
33. Ghayeb, H.H.; Hashim, A.R.; Ramli, S.N.H. Performance of Dowel Beam-to-Column Connections for Precast Concrete Systems under Seismic Loads: A Review. *Constr. Build. Mater.* **2020**, *237*, 117582. [\[CrossRef\]](#)
34. Zhao, H.; Peng, T.; Ge, P. Research on Damping and Restoring Force Performance of Artificial Hinge Based on the Micro-Nano Ceramic Coated Steel Bar. *Nanotechnol. Environ. Eng.* **2023**, *8*, 745–752. [\[CrossRef\]](#)
35. Zhao, H.; Yin, X. Seismic Mitigation and Self-Centering Performance of the Adaptive Structure Based on Artificial Hinge. *China Earthq. Eng. J.* **2022**, *44*, 1–9.
36. Zhao, H.; Yin, X. A Prestressed Assembled Artificial Hinge, Adaptive Damping Structure System and Its Construction Method. China Patent CN202121421652.4, 4 January 2022.
37. Santarsiero, G.; Picciano, V.; Masi, A. Structural rehabilitation of half-joints in RC bridges: A state-of-the-art review. *Struct. Infrastruct. Eng.* **2023**, 1–24. [\[CrossRef\]](#)
38. Li, Z.; Zhang, S.; Meng, Q.; Hu, X. Barriers to the Development of Prefabricated Buildings in China: A News Coverage Analysis. *Eng. Constr. Archit. Manag.* **2021**, *28*, 2884–2903. [\[CrossRef\]](#)
39. Luo, T.; Xue, X.; Wang, Y.; Xue, W.; Tan, Y. A Systematic Overview of Prefabricated Construction Policies in China. *J. Clean. Prod.* **2021**, *280*, 124371. [\[CrossRef\]](#)
40. Abaqus; Dassault Systèmes Simulia Corporation: Providence, RI, USA, 2014.
41. Bakhti, R.; Benahmed, B.; Laib, A.; Alfach, M.T. New Approach for Computing Damage Parameters Evolution in Plastic Damage Model for Concrete. *Case Stud. Constr. Mater.* **2022**, *16*, e00834. [\[CrossRef\]](#)
42. Alfarah, B.; López-Almansa, F.; Oller, S. New Methodology for Calculating Damage Variables Evolution in Plastic Damage Model for RC Structures. *Eng. Struct.* **2017**, *132*, 70–86. [\[CrossRef\]](#)
43. American Concrete Institute. *Building Code Requirements for Structural Concrete (ACI 318-19) and Commentary*; ACI: Farmington Hills, MI, USA, 2019; pp. 275–293.
44. Precast/Prestressed Concrete Institute. *PCI Design Handbook: Precast and Prestressed Concrete*, 8th ed.; PCI: Chicago, IL, USA, 2017; pp. 3.1–3.24.
45. Alshaikh, I.M.; Bakar, B.A.; Alwesabi, E.A.; Zeyad, A.M.; Magbool, H.M. Finite element analysis and experimental validation of progressive collapse of reinforced rubberized concrete frame. *Structures* **2021**, *33*, 2361–2373. [\[CrossRef\]](#)
46. Minh, H.L.; Khatir, S.; Wahab, M.A.; Cuong-Le, T. A concrete damage plasticity model for predicting the effects of compressive high-strength concrete under static and dynamic loads. *J. Build. Eng.* **2021**, *44*, 103239. [\[CrossRef\]](#)
47. Sümer, Y.; Aktaş, M. Defining parameters for concrete damage plasticity model. *Chall. J. Struct. Mech.* **2015**, *1*, 149–155.
48. Durand, R.; Vieira, J.F.; Farias, M.M. Numerical analysis of bonded and unbonded prestressed RC beams using cohesive and non-compatible rod elements. *Eng. Struct.* **2023**, *288*, 116157. [\[CrossRef\]](#)
49. Federal Emergency Management Agency. *HAZUS-MH MR4 Technical Manual*, 1st ed.; FEMA: Washington, DC, USA, 2003; pp. 9.17–9.18.

Disclaimer/Publisher’s Note: The statements, opinions and data contained in all publications are solely those of the individual author(s) and contributor(s) and not of MDPI and/or the editor(s). MDPI and/or the editor(s) disclaim responsibility for any injury to people or property resulting from any ideas, methods, instructions or products referred to in the content.